

Supporting Information

Adding refractory 5d transition metal W into PtCo system: An advanced ternary alloy for efficient oxygen reduction reaction

Yijun Wu, Yige Zhao, Jingjun Liu, Feng Wang**

State Key Laboratory of Chemical Resource Engineering, Beijing Key Laboratory of Electrochemical Process and Technology for Materials, Beijing University of Chemical Technology, Beijing 100029 (China)

E-mail: liujingjun@mail.buct.edu.cn (J. Liu), wangf@mail.buct.edu.cn (F. Wang)

Tel/Fax: +86-10-64411301

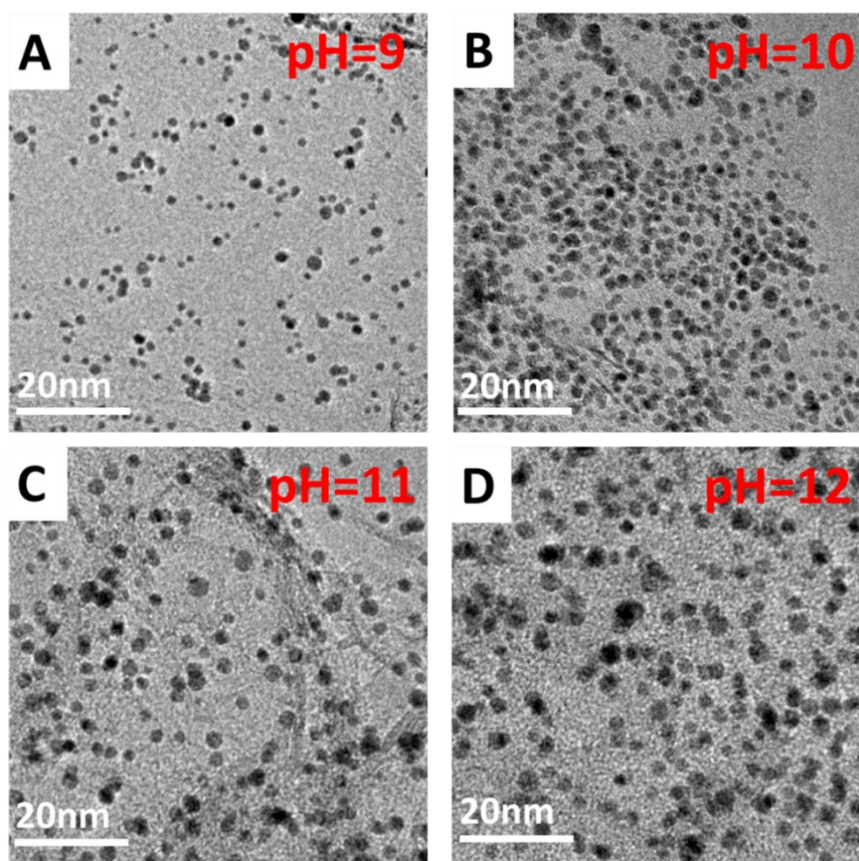


Fig. S1 Representative TEM images of the graphene-supported ternary Pt-Co-W alloy nanoparticles (Pt-Co-W/C) fabricated at different solution pH values: (A) pH=9; (B) pH=10; (C) pH=11; (D) pH=12.

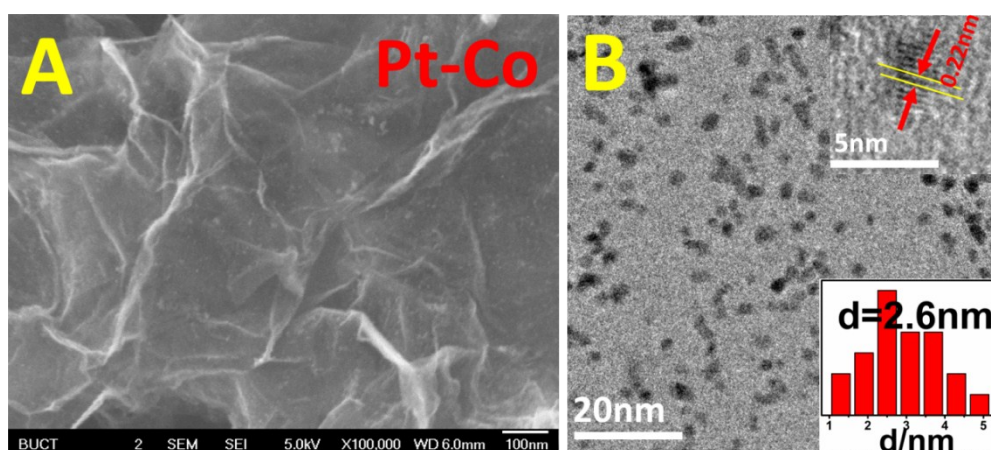


Fig. S2 (A) SEM image of the graphene-supported Pt-Co ternary alloy catalyst (Pt-Co/C); (B) TEM image of the graphene-supported ternary Pt-Co alloy nanoparticles, Insert: HRTEM image and the size distribution of Pt-Co alloy nanoparticles.

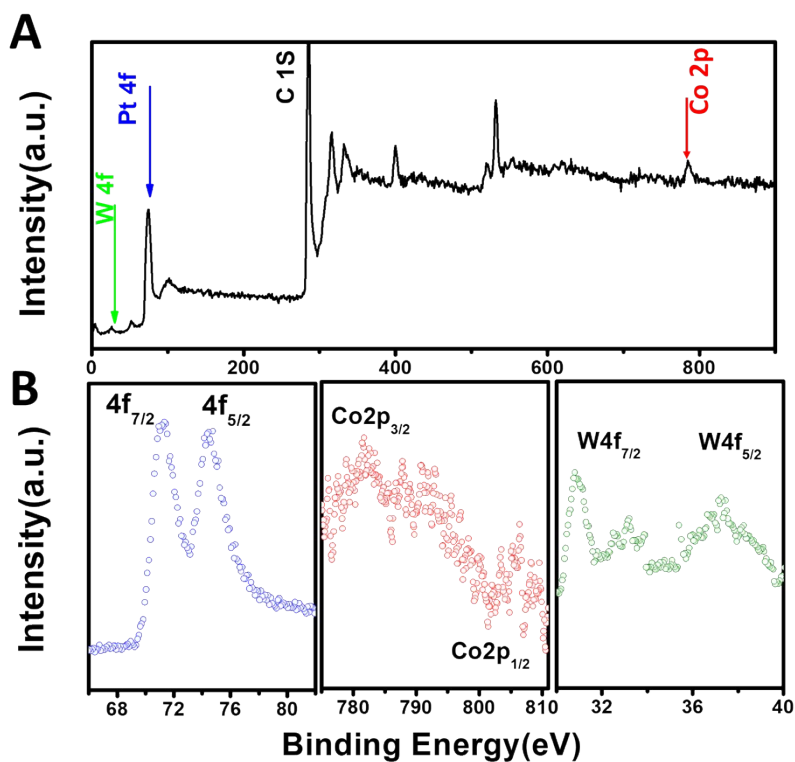


Fig. S3 (A) XPS survey for the Pt-Co-W catalyst. (B) Pt 4f, Co 2p and W4f XPS spectra. (the sensitivity factors of Pt 4f, Co 2p and W 4f are 15.46, 19.16 and 9.8, respectively.)

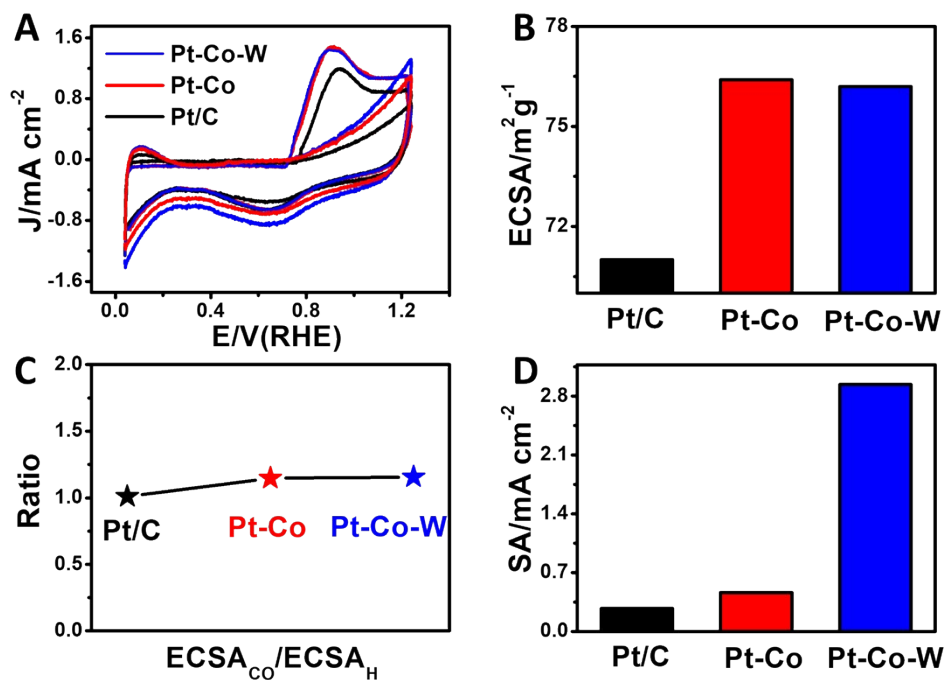


Fig. S4 (A) The CO stripping curves of Pt-Co-W, Pt-Co and commercial Pt/C catalysts

recorded at room temperature in CO-saturated 0.1 M HClO₄ solution. Scanning rate = 50 mVs⁻¹. **(B)** The electrochemically active surface area (ECSA) based on the CO stripping curves. **(C)** The ratio of ECSA values based on CO stripping (ECSA_{CO}) to those based on H_{upd} (ECSA_H). **(D)** The specific activities of the catalysts based on the above ECSA values at 0.9 V versus RHE.

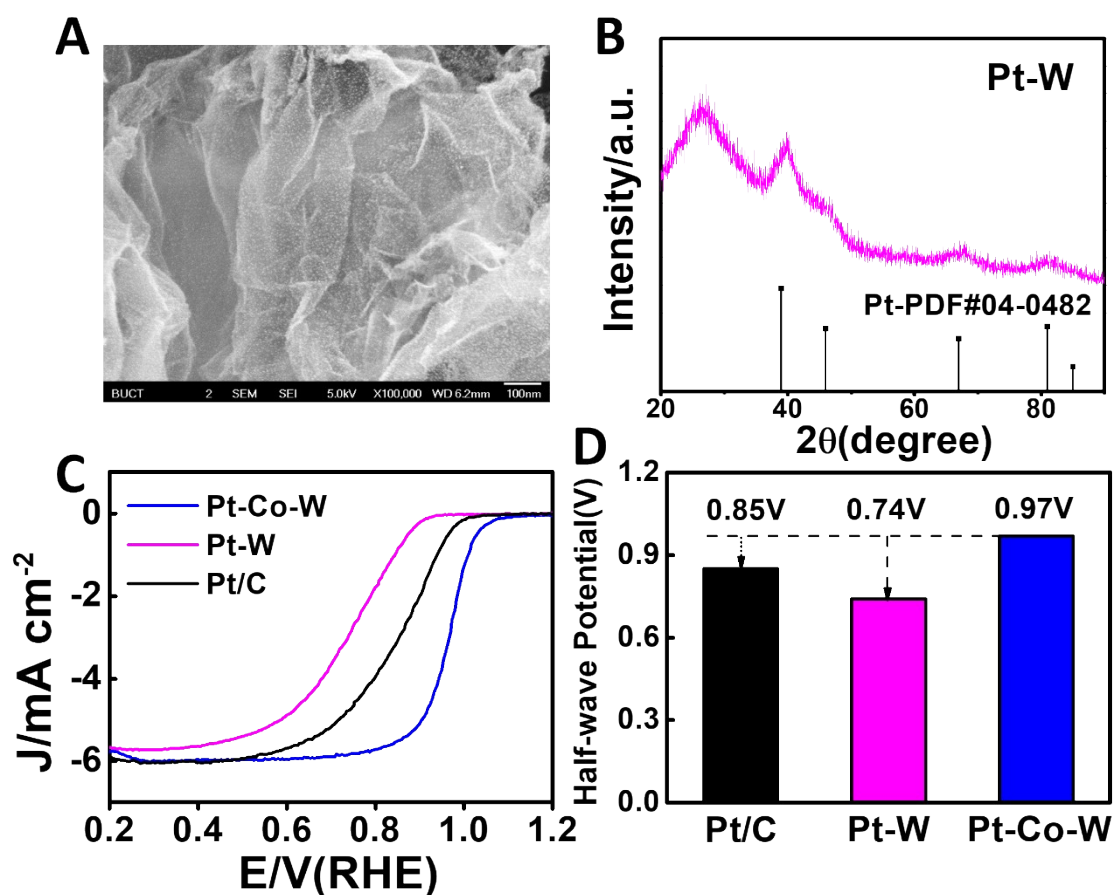


Fig. S5. (A) SEM image of Pt-W catalyst. (B) XRD patterns of Pt-W catalyst. (C) RDE measurements on Pt/C, Pt-W and Pt-Co-W catalysts in an O₂-purged 0.1M HClO₄ solution with a sweep rate of 5 mV·s⁻¹ at 1600 rpm; (D) The recorded half-wave potentials of Pt/C, Pt-W and Pt-Co-W catalysts.

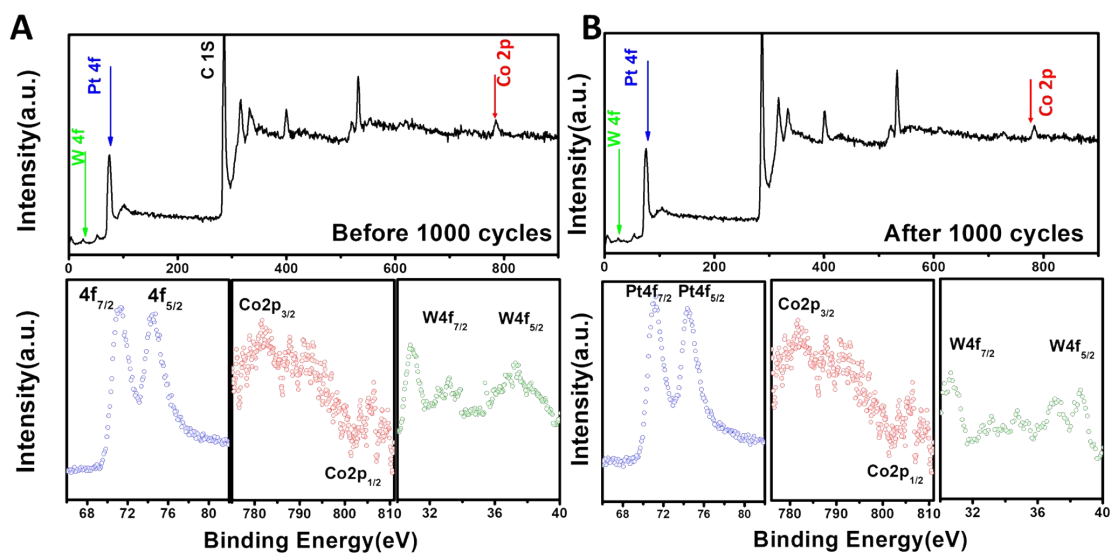


Fig. S6 XPS survey of Pt-Co-W catalyst and Pt, Co and W XPS spectra for the Pt-Co-W catalyst before (A) and after (B) 1000 cycles.

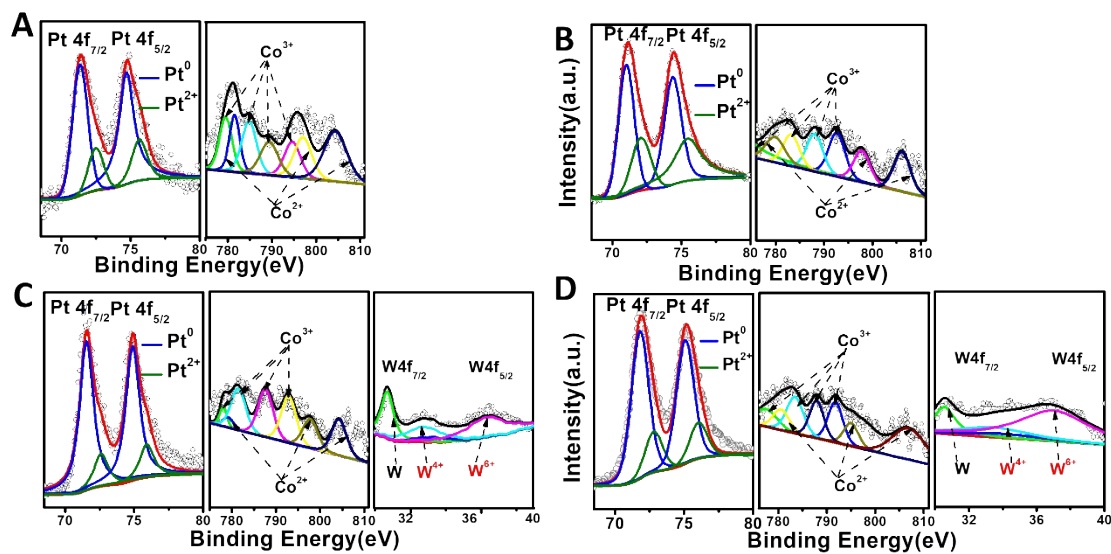


Fig. S7 Pt and Co XPS spectra for the Pt-Co catalyst before (A) and after (B) 1000 cycles in 0.1 M HClO₄ solution. Pt 4f, Co 2p and W 4f XPS spectra for the Pt-Co-W catalyst before (C) and after (D) 1000 cycles.

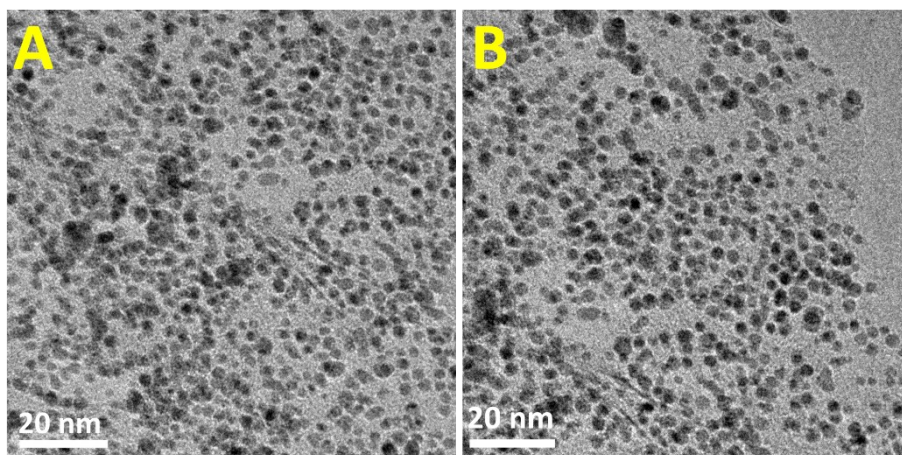


Fig. S8 TEM image of the graphene-supported ternary Pt-Co-W alloy nanoparticles, (A) before ADT; (B) after ADT.

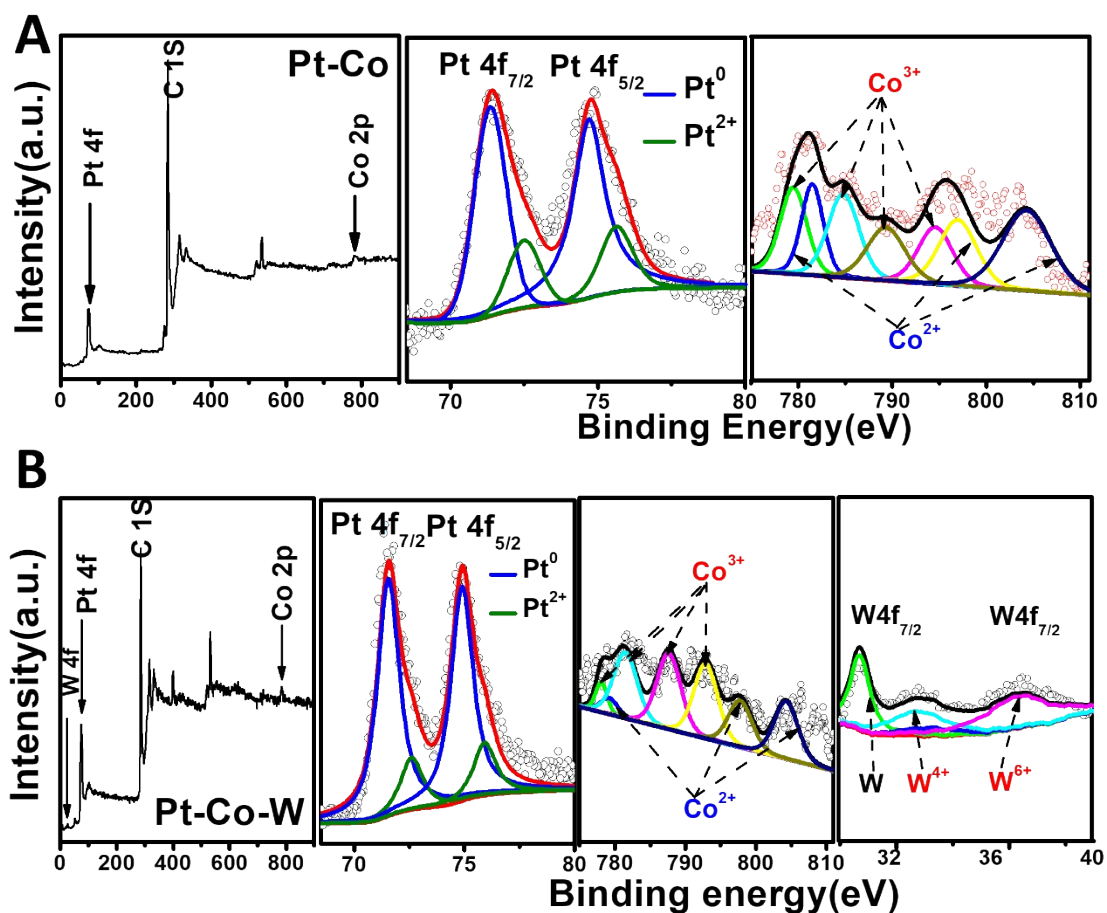


Fig. S9 (A) XPS survey, Pt and Co XPS spectra for the Pt-Co catalyst (B) XPS survey, Pt, Co and W XPS spectra for the Pt-Co-W catalyst.

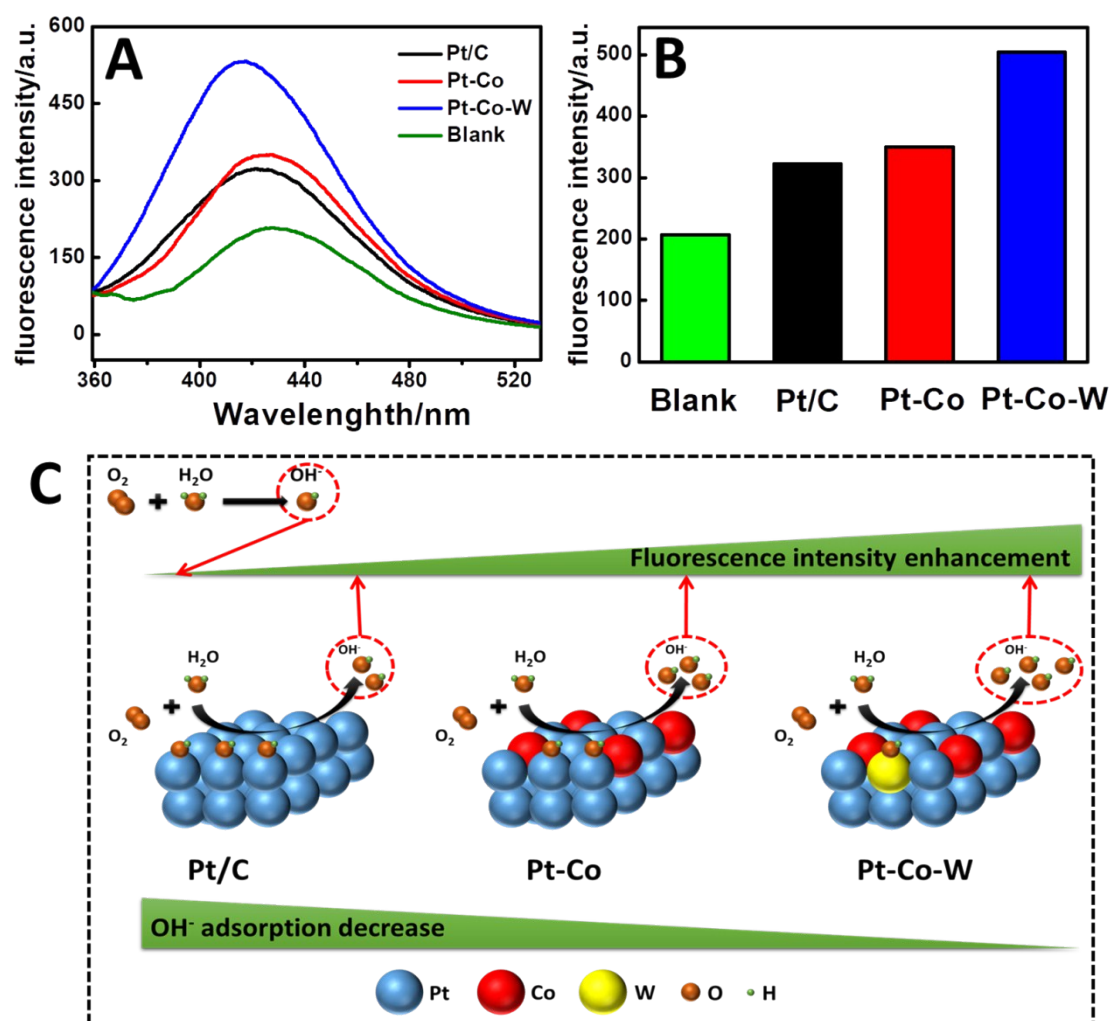


Fig. S10 (A) OH^\cdot trapping experiments: plots of the fluorescence spectral changes observed during microwave irradiation of different catalyst samples; (B) The fluorescence intensity of different catalyst samples at 426 nm; (C) Schematic illustration of the relation between the fluorescence intensity and the OH_{ads} desorption on the catalysts.

In order to provide a direct proof for the enhanced OH_{ads} desorption on the Pt-Co-W catalyst, the OH_{ads} trapping experiments on the Pt-Co-W catalyst, Pt-Co catalyst and commercial Pt/C were conducted. The OH_{ads} trapping experiment was conducted through the photoluminescence method by reacting terephthalic acid (TA) with OH^\cdot immediately to produce highly fluorescent products.⁵ As the concentration of TA is higher than 10^{-4} M, the TA is oxidized by OH^\cdot to produce highly fluorescent products. For the processes of OH^\cdot trapping experiments, 1 mg of Pt-Co-W catalyst (the same with other samples) was added into 50 mL of TA solution in a round flask and then subject to MW irradiation. At 2 min of intervals, 3 mL of reaction solution was sampled

and centrifuged to remove the catalysts for the subsequent photoluminescence analysis. Control experiments with catalysts and without any catalysts were conducted under the same conditions for comparison. In terms of this experiment procedure, firstly, the catalyst sample was added to an aqueous solution containing the terephthalic acid (TA). A small amount of oxygen in the solution was reduced to OH_{ads} with the help of the catalyst under microwave (MW) irradiation. Then the solution was centrifuged to obtain a supernatant. Given that the lifetime of OH_{ads} is too short to determine directly, the concentration of OH_{ads} in the supernatant was investigated through the highly fluorescent products (2-hydroxyterephthalic acid, TAOH, ex: 315 nm, em: 426 nm) produced by the reaction between terephthalic acid (TA) and OH_{ads} . So the fluorescence intensity is proportional to the OH_{ads} content in the supernatant in which the catalyst was removed. In other words, the higher the fluorescence intensity is, the more OH_{ads} exists in the supernatant. It indicates the residual OH_{ads} on the catalyst is less, suggesting that the OH_{ads} desorption of the catalyst is stronger. The fluorescence intensity of the different catalysts is shown in Fig. S10A, and the specific fluorescence intensity at 426 nm is shown in Fig. S10B. It can be seen that the fluorescence intensity of the Pt-Co-W catalyst is the largest relative to the Pt-Co catalyst and the commercial Pt/C, indicating that the residual OH_{ads} on the Pt-Co-W catalyst is the least, that is, the OH_{ads} desorption of Pt-Co-W catalyst is the strongest, as depicted in Fig. S10C. Thus, the above deduction about the enhanced OH_{ads} desorption on the Pt-Co-W catalyst is proved. In this work, the adsorption of O_2 on the Pt-Co-W catalyst is stronger than that of the Pt-Co catalyst, at the same time, the OH_{ads} desorption of the Pt-Co-W catalyst is further strengthened because the W atoms and OHs are easy to form W-OH ligand, giving lateral rejection to OH_{ads} absorbed on Pt skin. The catalytic activity of the Pt-Co-W catalyst is enhanced greatly compared to the Pt-Co binary catalyst.

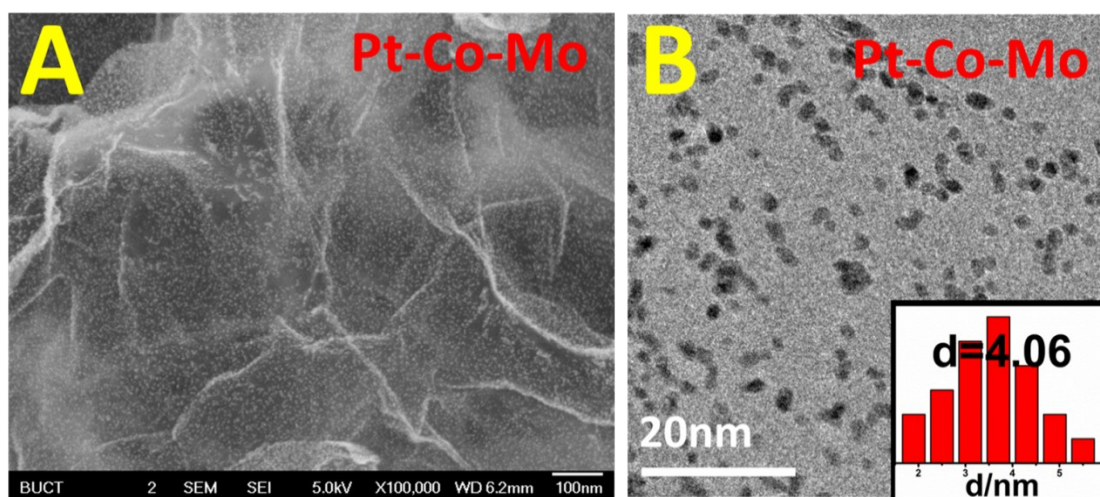


Fig. S11 (A) SEM image of the graphene-supported Pt-Co-Mo ternary alloy catalyst; **(B)** TEM image of the graphene-supported Pt-Co-Mo ternary alloy catalyst.

The obtained graphene-supported Pt-Co-Mo alloy nanoparticles are uniformly dispersed on graphene support, which can also be observed from the scanning electron microscope (SEM) and transmission electron microscope (TEM) image, as shown in Fig. S11A and Fig. S11B. As depicted by their corresponding particle size distribution histograms in the insets of Fig. S11B, the as-synthesized Pt-Co-Mo ternary alloy has a relatively uniform size distribution and their mean particle size is about 4.06 nm.

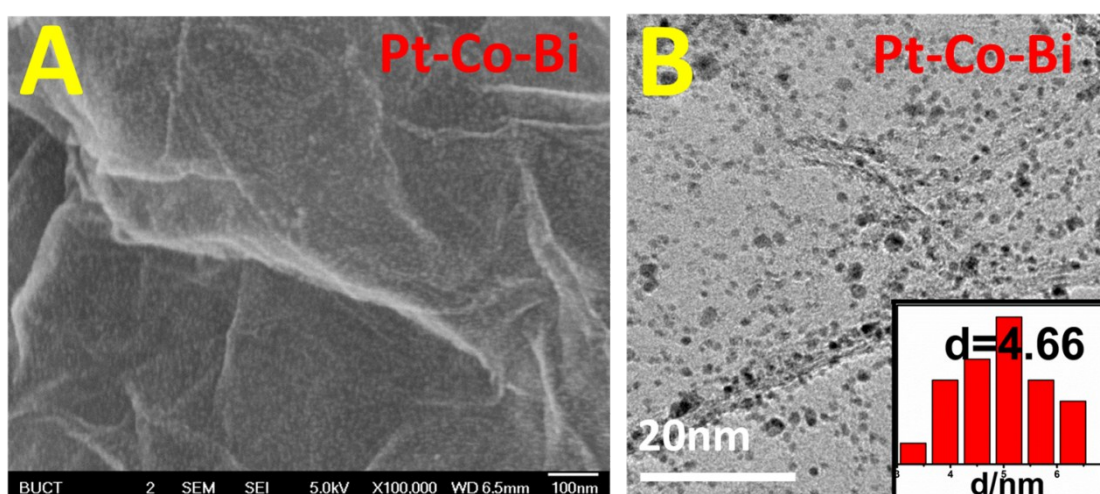


Fig. S12 (A) SEM image of the graphene-supported Pt-Co-Bi ternary alloy catalyst; **(B)** TEM image of the graphene-supported Pt-Co-Bi ternary alloy catalyst.

The obtained graphene-supported Pt-Co-Bi alloy nanoparticles are also uniformly dispersed on graphene support, as shown in Fig. S12A and Fig. S12B. As depicted by

their corresponding particle size distribution histograms in the insets of Fig. S12B, the as-synthesized Pt-Co-Bi ternary alloy has a reasonably uniform size distribution and the particle size is about 4.66 nm.

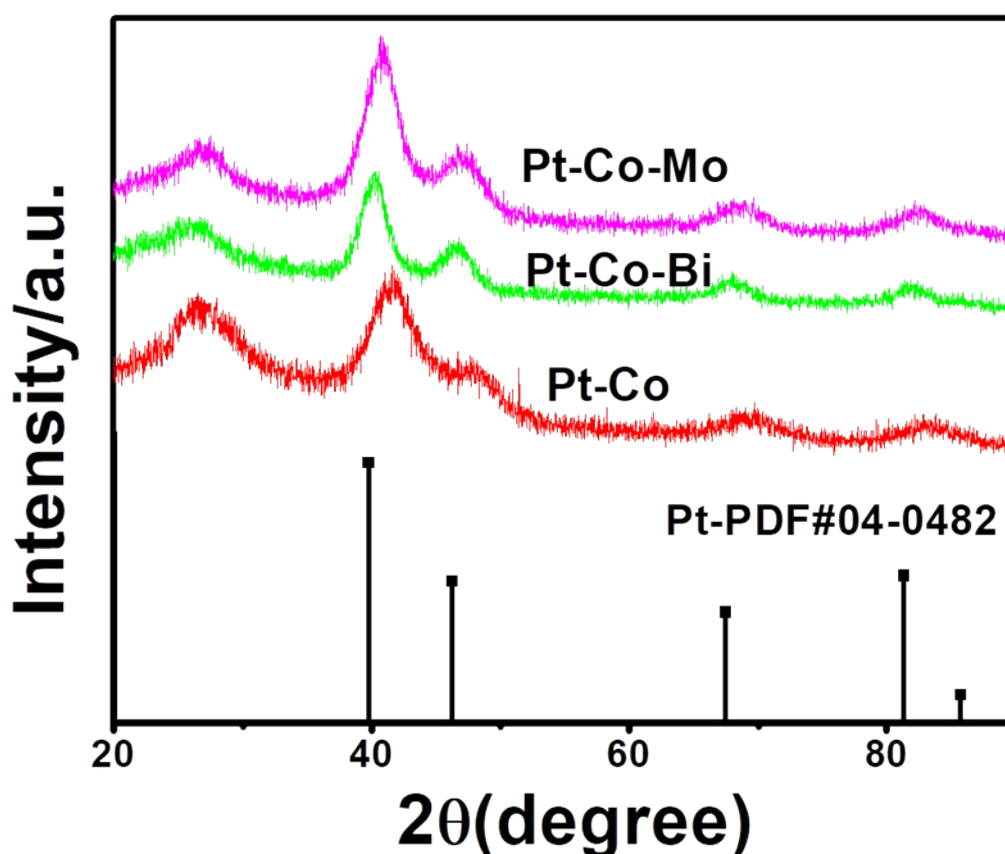


Fig. S13 XRD patterns of the graphene-supported Pt-Co-Bi and Pt-Co-Mo ternary alloys, with the Pt-Co binary catalyst as comparison.

The obtained XRD results are shown in Fig. S13, for the Pt-Co-Mo alloy, except for the carbon support peak at around 25°, the other four characteristic peaks correspond to the (111), (200), (220) and (311) planes characteristic of face-centered cubic (fcc) crystalline Pt (JCPDS number: 04-0802). No peaks of pure Co and Bi or other miscellaneous peaks are observed here. Moreover, compared with pure Pt, these characteristic peaks assigned to Pt-based alloy are obviously shifted to the higher angles, illustrating the formation of the Pt-Co-Mo solid solution alloy with a contractive state in lattice. A similar result has been found for the Pt-Co-Bi binary alloy shown in Fig. S13. However, because of the larger atomic radius of Mo and Bi atoms than that of Co atoms, there is a smaller shift of these characteristic peaks for the Pt-Co-Mo and

Pt-Co-Bi ternary alloy, relative to the Pt-Co binary alloy.

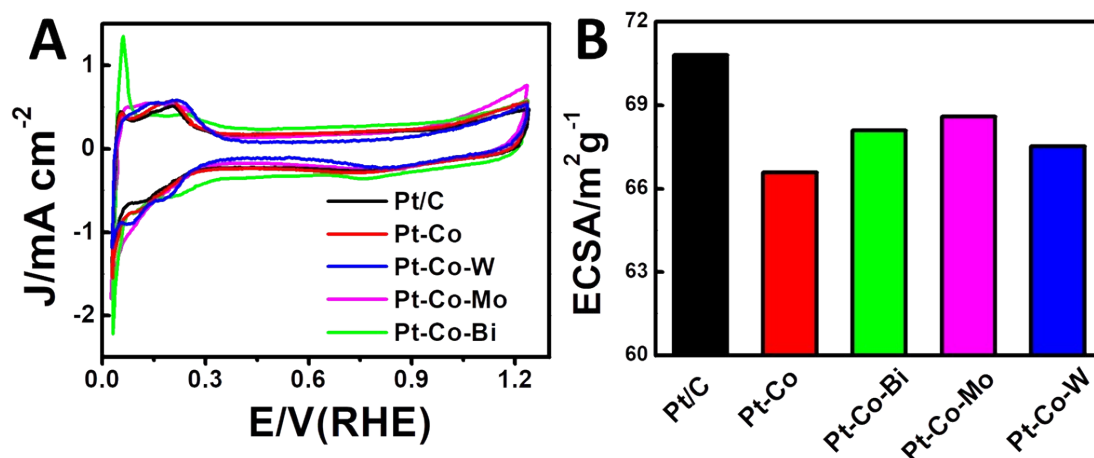


Fig. S14 (A) CV curves of all different catalyst samples in an N₂-purged 0.1M HClO₄ solution with a sweep rate of 50 mV·s⁻¹. (the current (J) is normalized by the area of the glassy carbon area (0.247 cm²)); **(B)** The measured specific ECSA of various catalyst samples.

Then cyclic voltammetry (CV) was used to measure electrochemically active surface areas (ECSAs) of all the catalysts (E-TEK, Pt-Co catalyst, Pt-Co-Bi catalyst, Pt-Co-Mo catalyst and Pt-Co-W catalyst) in an N₂-purged HClO₄ (0.1M) solutions at a sweep rate of 50 mV·s⁻¹. The obtained results of the above catalysts are shown in Fig. S14A. Based on the data in this figure, the ECSAs of the catalysts are calculated by the charge collected in the hydrogen adsorption/desorption region (between 0 V and 0.3 V) after double-layer correction and assuming a value of 210 μC·cm⁻² for the adsorption of a hydrogen monolayer.⁶ As depicted in Fig. S14B, the ECSA value of the Pt-Co-Bi (68.09 m²g⁻¹Pt⁻¹) and Pt-Co-Mo (68.58 m²g⁻¹Pt⁻¹) catalyst display similar and are between the ECSA value of Pt-Co-W catalyst (67.51 m²g⁻¹Pt⁻¹) and the ECSA value of Pt-Co catalyst (66.57 m²g⁻¹Pt⁻¹).

Table S1. Composition distribution of various Pt-based alloy catalysts

	Catalyst	Pt/molar%	Co/molar%	W/molar%
1	Pt-Co/C	72.1±0.2	27.9±0.7	0
2	Pt-Co-Bi/C	69.8±0.5	29.1±0.9	1.1±0.4
3	Pt-Co-Mo/C	72.1±0.5	24.4±0.3	3.5±0.3
4	Pt-Co-W/C	71.9±0.8	25.6±0.6	2.5±0.2

Table S2. The composition of Pt, Co and W components in the Pt-Co-W catalysts based on XPS and ICP results, respectively

	XPS	ICP
	Content (at%)	content (at%)
Pt	71.4	71.9
Co	25.9	25.6
W	2.7	2.5

Table S3. Catalytic activity of Pt-Co-W catalyst and some representative binary catalysts. (NA- not available; SA- Specific activity; MA- Mass activity; TW-This work).

Catalyst	Based on H _{upd}				Based on CO stripping			
	ECSA (m ² /g _{Pt})	SA (mA/cm ²)		MA (A/mg _{Pt})		ECSA (m ² /g _{Pt})	SA (mA/cm ²)	
		@0.9 V	@0.95 V	@0.9 V	@0.95 V		@0.9 V	@0.95 V
TW Pt-Co-W	65.9	3.41	0.97	2.25	0.64	76.4	2.94	0.86
TW Pt-Co	66.6	0.80	0.27	0.53	0.18	74.2	0.46	0.23
TW Pt/C	70.4	0.27	0.07	0.19	0.05	71.0	0.27	0.11
Ref.[1] Pt ₃ Co	NA	0.52	NA	1.10	NA	NA	NA	NA
Ref.[2] Pt ₃ Co	75.5	0.38	NA	0.21	NA	NA	NA	NA
Ref.[3] PtCu	NA	0.57	NA	NA	NA	NA	NA	NA
Ref.[4] Pt ₃ Ni	NA	1.2	NA	0.3	NA	NA	NA	NA

Table S4. The content of metals in the surface of catalysts before and after ADT test.

Relative intensities/%	Pt-Co-W	
	Original sample	Cycled sample
Pt	71.4	71.7
Co	25.9	24.9
W	2.7	3.4

Table S5 Relative intensities and FWHM of Pt 4f_{7/2} and Pt 4f_{5/2} peaks for various catalysts.

	Pt ⁰ relative intensities(%)		Pt ² relative intensities(%)		FWHM	
	4f _{7/2}	4f _{5/2}	4f _{7/2}	4f _{5/2}	4f _{7/2}	4f _{5/2}
Pt/C	43.9	32.1	13.3	10.7	2	2
Pt-Co	42.2	31.6	13.6	12.6	2.1	2.1
Pt-Co-W	43.0	31.9	12.7	12.4	1.9	1.9

Table S6. The contents of the alloy catalysts before and after ADT test.

	Before ADT			After ADT		
	Pt	Co	W	Pt	Co	W
Pt-Co	71.1±0.2	28.9±0.7	0	72.9±0.5	27.1±0.3	0
Pt-Co-W	71.4±0.8	26.1±0.6	2.5±0.9	71.9±0.1	26.0±0.4	2.1±0.7

References

1. Y. Xu, A. V. Ruban, M. Mavrikakis, *J. AM. CHEM. SOC.*, 2004, **126**, 4717-4725.
2. Y. G. Zhao, J. J. Liu, C. G. Liu, Y. Song and Wang, *F. J. Mater. Chem. A*, 2015, **3**, 20086-20091.
3. E. J. Coleman, M. H. Chowdhury and A. C. Co, *ACS Catal.*, 2015, **5**, 1245-1253.
4. J. Zhang, H. Yang, J. Fang, S. Zou, *Nano Lett.*, 2010, **10**, 638-644.
5. Y. L. Chen, Z. H. Ai and L. Z. Zhang, *J. Hazard. Mater.*, 2012, **92**, 235-236.
6. X. Q. Huang, Z. P. Zhao, *Science*, 2015, **348**, 1230-1234.